Determination of Secondary Species in Solution Through Pump-Selective Transient Absorption Spectroscopy and Explicit-Solvent TDDFT

M. A. P. Turner,[*,†,‡,¶] M. D. Horbury,[†] V. G. Stavros,[†] and N. D. M. Hine[*,‡]

†*Department of Chemistry, University of Warwick, Coventry, CV4 7AL*

‡*Department of Physics, University of Warwick, Coventry, CV4 7AL*

¶*Current address: Top Floor Senate House, University of Warwick, Coventry, CV4 7AL*

E-mail: m.turner.1@warwick.ac.uk; n.d.m.hine@warwick.ac.uk

Abstract

The measured electronic excitations of a given species in solution are often a composite of the electronic excitations of various equilibrium species of that molecule. It is common for a proportion of a species to deprotonate in solution, or form a tautomeric equilibrium, producing new peaks corresponding to the electronic excitations of the new species. One prominent example is alizarin in methanol, which at different temperatures, and in solutions with differing pH, has an isosbestic point between the two dominant excitations at 435 nm and 540 nm. The peak at 435 nm has been attributed to alizarin; the peak at 540 nm, however, more likely results from a species in equilibrium with alizarin. In this work, we were able to use both experimental and computational techniques to selectively examine electronic properties of both alizarin and its secondary species in equilibrium. This was achieved through use of transient electronic absorption spectroscopy, following selective photoexcitation of a specific species in equilibrium. The resulting transient electronic absorption spectra were compared to the known transient absorption spectra of potential secondary equilibrium species. The ground state absorption spectra associated with each species in equilibrium were predicted using linear-scaling Time-Dependent Density Functional Theory with an explicitly-modelled solvent and compared to the experimental result. This evidence from both techniques combines to suggest that the excitation at 540 nm arises from a specific monoanionic form of alizarin.

Introduction

The optical absorption spectrum of a molecule in solution often comprises of a superposition of spectra originating from several different species, each arising from the equilibrium process associated with a given parent molecule.[1,2] For example, tautomeric equilibria and equilibrium between possible charge states will produce a wide range of species each providing different contributions to the total spectrum. These equilibrium species may result in unwanted effects, for instance in medicine where potentially dangerous side products may be

formed,[3] or in dyes or paints whose colour may be affected by properties which influence the equilibrium, such as solvent, pH, or temperature.[4] Determining the identity of the various species present is the first step to controlling them, but is currently challenging both for experimental and theoretical methods. In this paper we apply a combination of state-of-the-art experimental and theoretical techniques to deconvolve the spectrum of a widely studied exemplar dye, namely Alizarin. Alizarin is a common dye used frequently for biological staining of cells, bones, and cartilage[5,6] as well as for studying inorganic processes like the growth of TiO_2 nanotubes.[7] It has been subjected to experimental[8,9] and computational[10–19] studies with a wide range of techniques, but as we show here, the identity of the main secondary absorption peak in protic solvents has not previously been unambiguously determined. Here we use a combination of methods that enables definitive identification of peaks, pointing the way to increased feasibility of Ultraviolet-Visible (UV-Vis) based tools for analysis of organic compounds in a range of solvents.

Figure 1 shows the UV-Vis spectrum of alizarin in a selection of common solvents. When alizarin is dissolved in non-protic solvents, the resulting spectrum displays only one major peak, at approximately 435 nm, which we call excitation α. However in protic solvents such as methanol, and to a lesser extent ethanol, a clear secondary peak is present at approximately 540 nm, which we call excitation β. As it represents the clearest example of this secondary excitation, we elect to study alizarin in methanol as an exemplar system for secondary species determination. UV-Vis spectra of alizarin in methanol taken at varying temperatures show a clear decrease in absorption for excitation α and increase in absorption for excitation β as temperature increased (see supplementary information Fig S1). A clear isosbestic point is present between the two excitations, implying that the secondary excitation is not the result of a lower-energy electronic excitation of the highest-concentration species of alizarin, but rather is likely due to the presence of a secondary species of alizarin whose concentration varies with temperature. This peak has been observed previously, and has prompted debate as to whether it corresponds to a monoanionic form of alizarin or a tautomer.[12,14,20] Figure

2 parts (A), (B), (C), and (D) enumerate the candidate species we consider in this work.

Le Person *et al.* concluded that this excitation was due to both monoanionic alizarin and the alizarin-b tautomer.[20] Others in the literature however question the presence of the alizarin-b tautomer in methanol, instead suggesting that the β excitation is entirely caused by different tautomeric and rotameric monoanionic species.[11,14,21] In some cases where there is a need to distinguish secondary species, nuclear magnetic resonance can be a good option. However, in this system the rate in which the equilibria species inter-converted is too fast for them to be distinguishable. In other situations, infrared based techniques are ideal. However, for this combination of solvent and solute, the vibrational frequencies of interest, specifically those arising from the hydroxyl groups, are also present in the methanol solvent, causing the signal to be eclipsed. The use of deuterated solvent can be ruled out owing to the fast exchange of hydrogen/deuterium between solute and solvent. The unclear overall situation thus suggests alizarin as an ideal testing ground for novel approaches to determining the identity of secondary species.

Two complementary techniques are required for an unambiguous species determination: high-accuracy theoretical spectroscopy on each candidate species, and species-selective 'fingerprinting' *via* time-resolved spectroscopy. We achieve the necessary accuracy in theoretical spectroscopy by using a newly-emerging combination of methodologies: linear-scaling time-dependent DFT[22,23] and spectral warping.[24] The reduced scaling of the computational effort associated with linear-scaling forms of linear-response Time-Dependent Density Functional Theory (TDDFT)[25] enables calculations on an ensemble of model systems each incorporating a large solvent cluster, as has been shown to be necessary to fully converge the solvatochromic shift.[23] Meanwhile spectral warping[24] enables excitation energies calculated with a computationally 'cheap' density functional, allowing high-throughput calculations but relatively limited overall accuracy, to be transformed by a simple predetermined warping function to produce results equivalent to calculations using a much higher-accuracy, but correspondingly expensive, state-of-the-art functional. The combination of these techniques has been shown

4

to enable accurate colour prediction of dyes exhibiting strong solvatochromism resulting from various competing effects.[13] In the current work it can be used to predict the excitation energies from each species in a given solvent, which can be compared to experimental spectra to determine the likely concentration of each of the candidate molecules. However, it has also been observed that with the available accuracy of even state-of-the-art exchange-correlation (xc) functionals, confidence in theoretical colour prediction can be difficult to obtain, due to the spread of results obtained for different functionals. Therefore, in this work, we use alignment with the known experimental spectra for the majority species to eliminate the main part of the functional-dependent error, resulting in close alignment of the predicted secondary peaks.

To enable even greater confidence in the identity of equilibrium species giving rise to specific absorption peaks, we also examine their excited state properties. Experimentally, these are assessed *via* transient electronic absorption spectroscopy (TEAS), commonly used to probe excited state decay in molecules.[26–28] In this work, the pump wavelength was specifically selected to excite the α and β excitations separately. The resulting excited state dynamics were then compared to excited state dynamics of a buffered solution certain to contain the monoanionic form of alizarin.

Methodology

Experimental methodology

All steady state UV-Vis measurements were taken on the a Cary 60 spectrophotometer. Alizarin (SIGMA-ALDRICH, 97 %) was dissolved in spectroscopy grade methanol (3 μM). This solution was used for all studies aside from the UV-Vis spectra taken in other solvents in Figure 1, for which the concentration used was also 3 μM. Buffer solutions were made for the pH 3 buffer with trichloroacetic acid (ACS Reagent, SIGMA-ALDRICH, 99.5 %) and sodium trichloroacetate (SIGMA-ALDRICH, 97 %). The pH 7 buffer was made using acetic acid
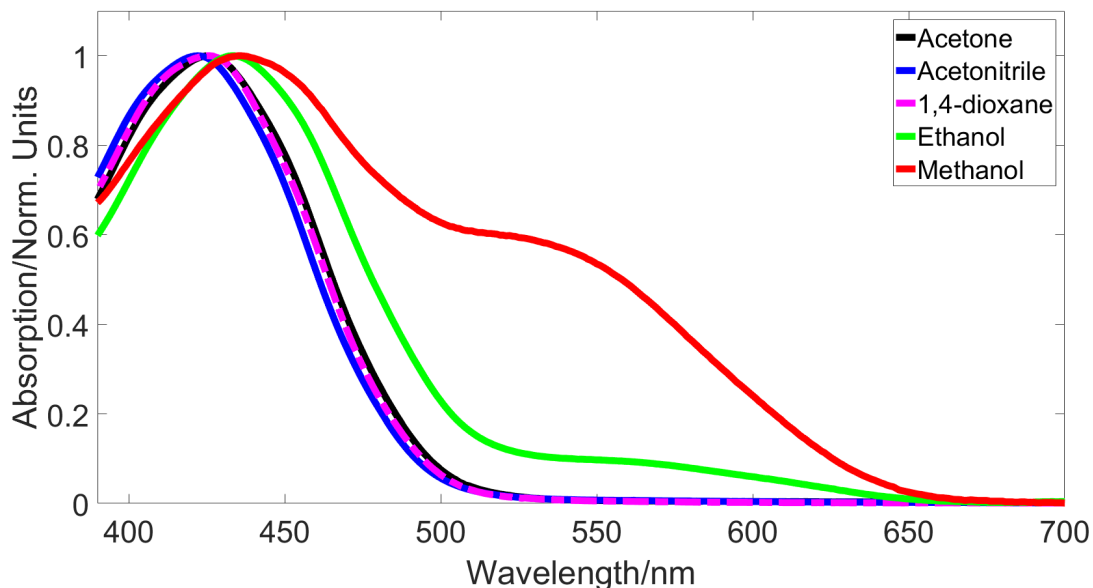
Figure 1: UV-Vis spectra of alizarin in different solvents. A prominent shoulder is observed in methanol, and to a lesser extent in ethanol, at around 540nm

(SIGMA-ALDRICH, 97 %) and sodium acetate (SIGMA-ALDRICH, 99 %). Buffers were made by dissolving reagents in methanol, the concentrations of each component is shown in Table 1. The components were mixed in a 4:1 acid to salt ratio, although these were calculated using approximate pK_a values so the pH was corrected by adding components dropwise until at the right pH, monitored using pH paper. This was due to difficulty with using electrochemical probes in organic solution. The basic alizarin was made by adding aqueous sodium hydroxide. This was not a buffer owing to the safety issues surrounding making basic buffers in methanol. The pH was regularly monitored and did not deviate from approximately 9 therefore we believe this method to be reliable.

Table 1: **Starting concentrations for making pH buffers.**

Buffer component	Concentration/mM
Trichloroacetic acid (pH=3 buffer)	2.27
Sodium trichloroacetate (pH=3 buffer)	27.0
Acetic acid (pH=7 buffer)	24.1
Sodium acetate (pH=7 buffer)	1.4

The transient electronic absorption spectroscopy set up is the same as used in several
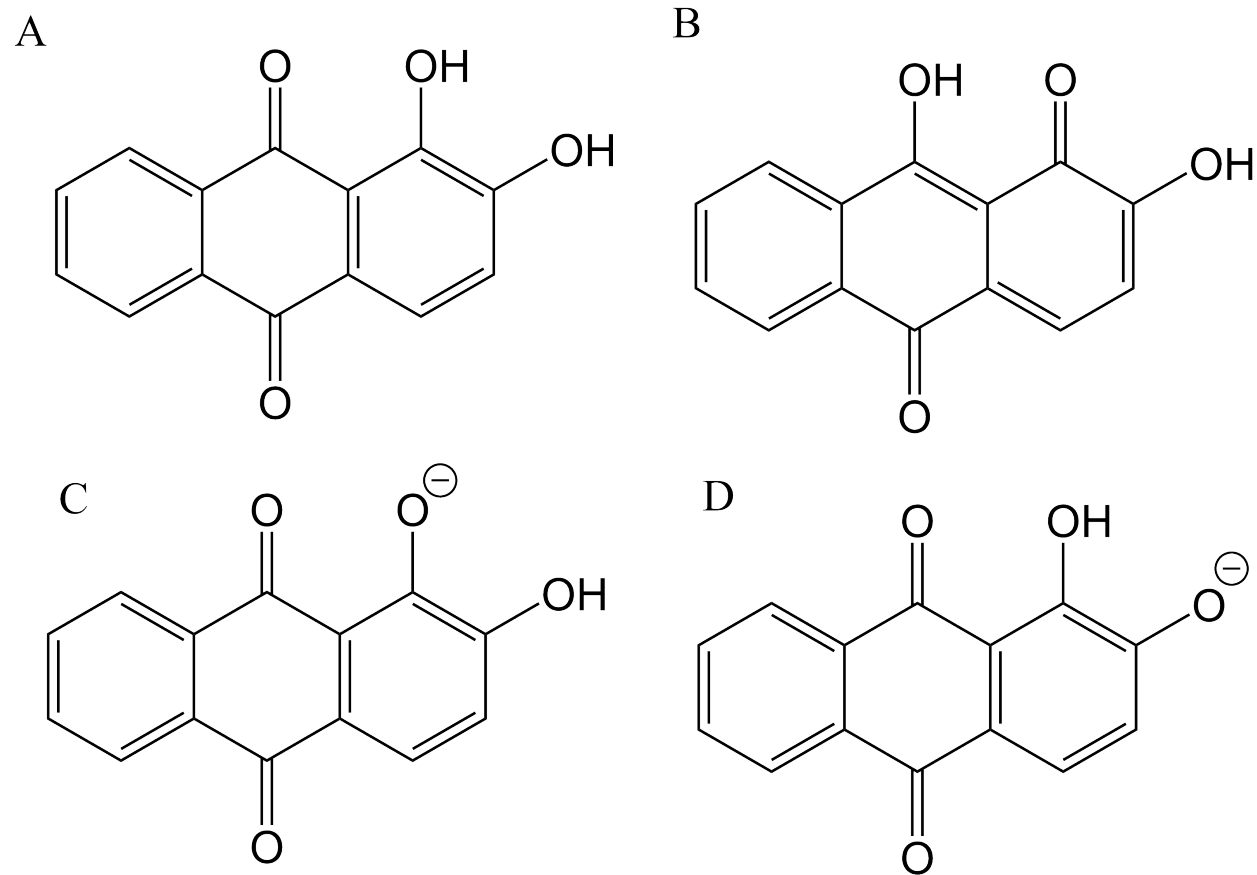
Figure 2: The primary (A) and secondary (B-D) structures considered within this work. A) Alizarin-a tautomer B) Alizarin-b tautomer C) Alizarin monoanion-a D) Alizarin monoanion-b.

previous works, including Greenough *et al.* and Horbury *et al..*[29–31] The concentration of alizarin in each solution was increased to 0.1 mM. The broadband probe pulse was generated through focusing 800 nm incident light on a 2 mm CaF_2 window, this was translated vertically, and spanned a spectral region of 345 nm to 675 nm. The femtosecond (fs, 10^{-15} s) pump pulses were produced using an optical parametric amplifier (TOPAS-C, spectra-physics). The pathlength used for each scan was 100 μm and the fluence was $\approx$ 1-2 mJcm^{-2}, the appropriate pump wavelengths are stated in the text. The absorption at 100 μm pathlength was 0.045 OD. The instrument response of the TEAS measurements was retrieved by fitting Gaussians to the time-zero artifacts present in the solvent scans in the acidic and neutral solutions (MeOH and buffer only solutions, see figure S5) and taking the full width half maximum; this gave a value of $\approx$ 80 fs.

Computational methodology

For LR-TDDFT calculations in vacuum and in implicit solvent, we use the NWChem package.[32] We have employed the cc-pVTZ basis set and performed a full geometry optimisation for each combination of functional and environment unless otherwise stated.[33] For implicit solvent calculations we use the COSMO model[34–36] as implemented in NWChem, with dielectric parameters set to represent the methanol environment.

For explicit solvent calculations, to generate an ensemble of realistic configurations of the molecule immersed in methanol solvent, we first perform molecular dynamics calculations with the AMBER package.[37] Force field parameters for each molecular species were generated using the antechamber tool, in their DFT-optimised geometry.[38] The molecules were then placed in a box of methanol of side length 20 Å. The generalised Amber force field (GAFF)[39] was used to first conduct an energy minimisation of the box and then to equilibrate the box by raising the temperature up to 300 K over the course of 3 fs. Following this, the box was maintained *via* a Langevin thermostat at a constant temperature of 300 K over the course of 2 ps, during which 60 snapshots were extracted at regular time intervals. This procedure

is thus imagined to generate statistically-independent set of snapshot representations of the box.

A spherical region of the periodic box is then extracted, of a fixed radius centered on the centre-of-mass of the target molecule. The required radius of this region is chosen to balance a desired degree of convergence of the solvatochromic shift against increasing computational cost as the sphere radius is increased. The principal hydrogen bonding interactions would occur for solvent molecules within 2.5 Å of the solute, while electrostatic interactions originating from the solvent dipoles will fall off rapidly with increasing distance. Based on previously-reported studies,[40] we determined that the solvent sphere can in this case be truncated to a radius of 10 Å. The usage of implicit solvent model[41] surrounding the explicit solvent shell was necessary in order to correctly screen the surface dipoles and prevent a net dipole across the solvent cluster. This is in agreement with previous work[42] which showed that an appropriate treatment of the electrostatics of solvent clusters is necessary to retain physically-reasonable behaviour of the HOMO-LUMO gap. Truncation of radius 10 Å produced models of typical size 500-600 atoms (the exact number is dependent on the specific configuration of the snapshot), which is beyond the capabilities of traditional approaches to LR-TDDFT calculations.

For LR-TDDFT calculations on the solvent and solute clusters, we therefore utilise the ONETEP Linear-Scaling Density Functional Theory package.[43] ONETEP uses a representation of valence, conduction and transition density matrices in terms of localised support functions referred to as Non-orthogonal Generalised Wannier Functions (NGWFs). A minimal number of NGWFs per atom (here four per C and O atom, and 1 per H atom), strictly localised to a sphere of a given radius (here 10 Å), are expressed in terms of an underlying basis of psinc functions (equivalent to plane-waves, with a cutoff energy of 800 eV in this case) and are optimised in-situ during the calculation. Density kernel and NGWF optimisation is applied separately to valence and conduction NGWF sets,[44] then the combined 'joint' set is used for LR-TDDFT calculations within a modified version Casida formalism[25]

adapted for the linear-scaling framework.[22,23] The first five LR-TDDFT excited states are found for 60 snapshots for each candidate species, utilising the PBE[33] exchange-correlation functional.

While, PBE calculations are not expected to provide quantitatively accurate spectra, it is expected that they will provide an accurate representation of the solvent-induced broadening and solvent-solute specific interactions. In order to then obtain more accurate results for the ensemble of solvent-solute clusters within feasible computational effort, spectral warping was applied. This is a technique devised by Ge *et al.* which aims to reproduce the accuracy associated with hybrid functionals by correcting results obtained for an ensemble of large models treated using a less expensive semi-local functional.[24] For each of the candidate species, otherwise-identical LR-TDDFT calculations were performed with several functionals: PBE, B3LYP and PBE0 (global hybrids) and CAM-B3LYP and LC-PBE (range separated hybrids) in their relaxed gas phase geometry. A linear transformation of the energies associated with each excitation is then constructed, which maps the PBE results onto the (range-separated) hybrid functional result. This same linear transformation can then be applied to each of excitations from the explicit solvent snapshots, to approximately reproduce the effect of using the hybrid functional on the full cluster.

Results and discussion

Acid/Base UV-Vis studies

Alizarin in methanol was buffered at pH 3 and pH 7 using methanol-based buffers as described in the methodology section. Alizarin in methanol was also studied at pH 9 through addition of sodium hydroxide in water. UV-Vis spectra were taken at each pH value, and are shown in Figure 3. When buffered to pH 3 the β excitation is no longer present. We suggest that, as there is likely no monoanion at pH=3, the β excitation was a result of a monoanionic species. However, one could argue that alizarin-b is stabilised in methanol through hydrogen bonding

10

and this is perturbed by addition of acid. Alternatively, the buffer could be reacting in order to remove alizarin-b, although this is less likely as no signs of a reaction are evidenced by decolouration or the appearance of new features not present in the original spectrum. Under basic conditions, the α excitation decreases as the alizarin-a is largely deprotonated. At around 469 nm there is an isosbestic point, which lends further credence to the theory that an equilibrium between two species is observed. This occurs close to where Miliani *et al.* observed an isosbestic point, 463 nm when alizarin was dissolved in water. This further supports that the same equilibrium is forming.[12] From this evidence, it is highly likely that monoanionic alizarin is present in neutral methanol and is responsible for a peak at 540 nm.
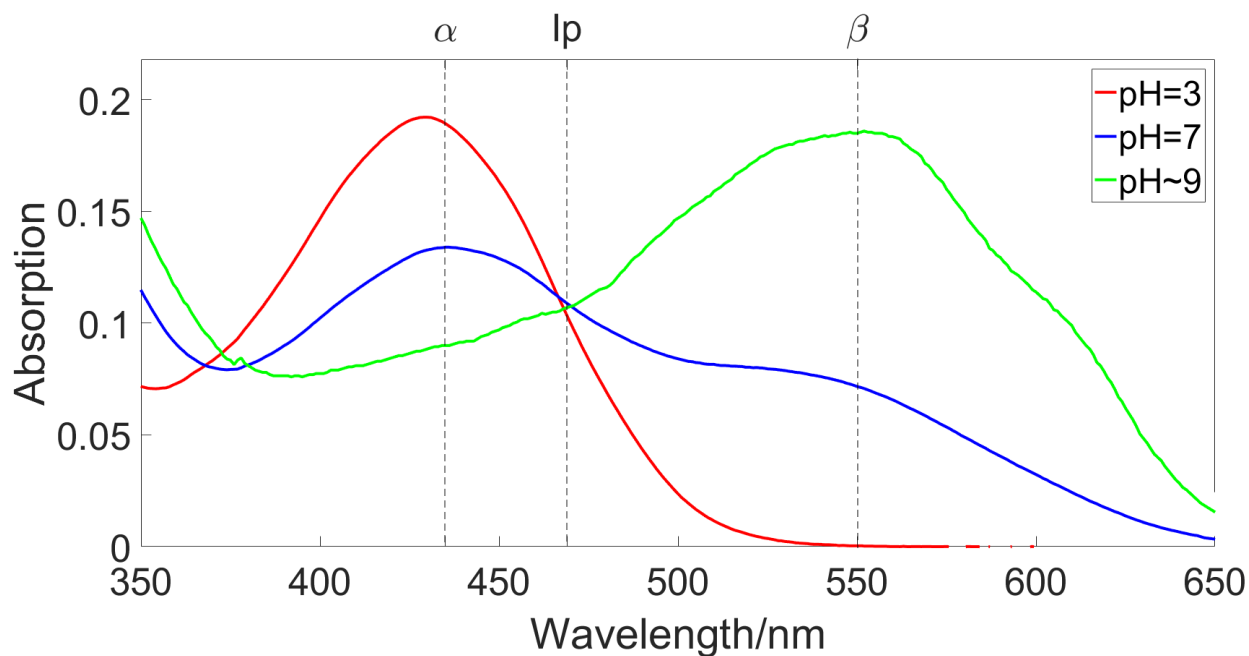

Figure 3: Alizarin in methanol at various pH values: (red line) buffered to pH 7 using an acetate buffer; (blue line) buffered at pH 3 using a trichloroacetate buffer; (green line) pushed to pH 9 through addition of NaOH(aq). The dotted line (Ip) shows the position of the isosbestic point.

Transient electronic absorption spectroscopy results

Transient electronic absorption spectroscopy is a useful technique for verifying that the features present in the transient absorption spectra for samples with different solvent environ-

ments (pH in this case) share a common photoactive species. We can use a combination of two indicators within the transient absorption spectra as a two-tier identification process for the photoactive species. Firstly, one can observe whether the same spectral features appear, such as stimulated emission and excited state absorption occur at the same pump wavelength λ_{ex}. Secondly, one can observe whether the different samples have similar temporal evolution of these excited state features as well as decay pathways. This can be especially useful to confirm that there is not a mix of species being probed, as this would lead to the superposition of multiple decay pathways in the time-resolved responses of the different samples. Using this two-tier identification, if different samples have the same features that evolve in the same temporal manner in their transient absorption spectra, it is very likely the same photoactive species is present.

Transient electronic absorption spectra of alizarin in methanol were taken with the photoexcitation (or pump) pulse at 425 nm, near excitation α, and 550 nm, near excitation β. These wavelengths were chosen to excite the individual species as much as possible without exciting the tail of the other form. These were conducted under acidic, neutral, and basic conditions, see Figure 4. When exciting at 425 nm under acidic and neutral conditions, Figures 4a and 4b, we see very similar features, with an excited state absorption at 500 nm and a stimulated emission at 675 nm. This due to the fact that in both cases alizarin a is excited by the pump pulse. There are similarities in the transient electronic absorption data when exciting at 550 nm under basic and neutral conditions, Figure 4c and Figure 4d, as well. This is interesting as the species excited under basic conditions is very likely a monoanionic form. This is due to the fact both alizarin-a and alizarin-b will deprotonate in a basic environment, as evidenced by earlier UV-Vis studies. As the results for Figure 4c and Figure 4d show such similar features, with two excited state absorption features at 390 nm and 450 nm and a stimulated emission at 550 nm, it is likely that in both cases a monoanionic form of alizarin is excited.
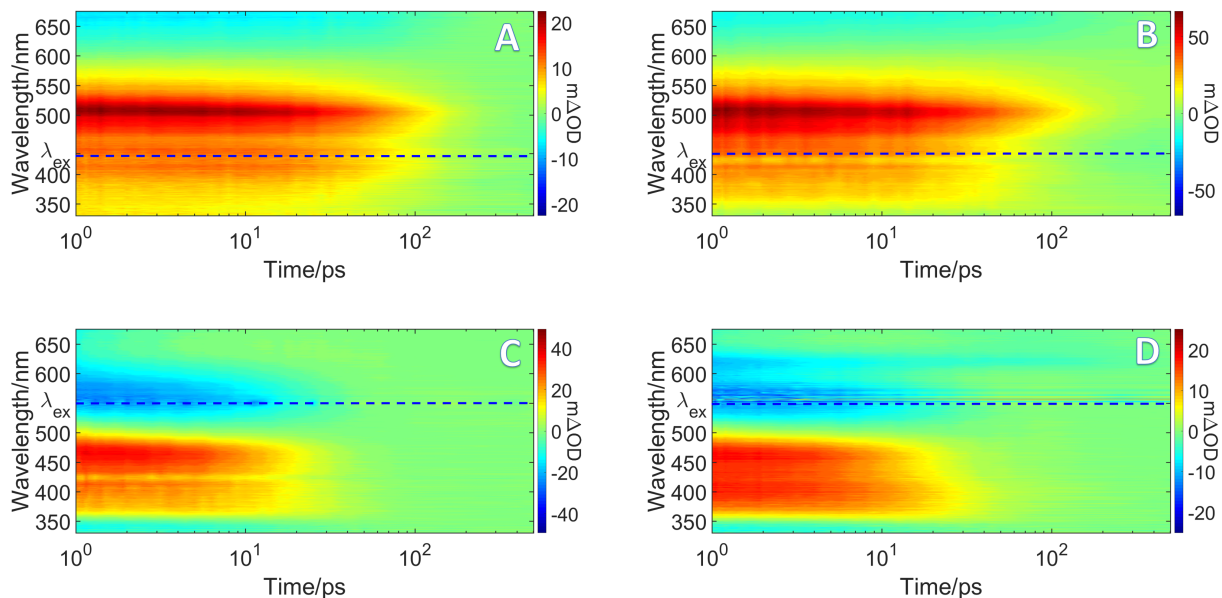
Figure 4: TEAS of alizarin in methanol (0.1 mM). The blue dashed line on each plot represents the excitation wavelength. a) pH=3, λ_{ex}=425 nm; b) pH=7, λ_{ex}=425 nm; c) pH=7, λ_{ex}=550 nm; d) pH=9 λ_{ex}=550 nm.

The excited state absorption features observed were fitted with a bi-exponential decays, these were convolved with Gaussian curves to account for instrument response. Whilst each appeared to have a mono-exponential character, a second exponential is necessary to account for the different, smaller scale, short-time effects, such as vibrational cooling. These features were normalised by pump power. Plots of each of these fitted features are in Figures S2 and S3 with the lifetimes of features shown in Table 2.

Table 2: Lifetimes extracted from fitted curves for the excited state features of alizarin observed.

pH	λ_{ex}/nm	λ_{pr}/nm	Lifetime (τ_1)/ps	Lifetime (τ_2)/ps
3	425	500	< 0.04	120 ± 21
7	425	500	< 0.04	94 ± 4
7	550	460	0.41 ± 0.05	15.8 ± 0.5
9	550	460	0.4 ± 0.1	17 ± 1

Each of the scans at 425 nm had a long lifetime decay in the order of approximately 100 ps as well as a decay <40 fs, therefore within our instrument response. This result is similar to what was observed by Lee et al. when observing the ultrafast dynamics of alizarin

with an excitation wavelength of 403 nm in ethanol.[45] Lee et al. observed two lifetimes for alizarin, one at 84 ps and one at 3 ps. We did not pick up on the 3 ps lifetime, likely due to its low intensity, but it is likely that we are observing the same long-lived decay of alizarin-a. Lee et al. suggested that the process responsible for this lifetime was proton-transfer and the formation of alizarin-b in the excited state. The amplitude of the long-lived process was significantly higher than that of the short-lived by a factor of approximately 30 in each case.

The scans at 550 nm show two decays, one of approximate lifetime 16 ps and one of approximate lifetime 400 fs. Again, the long-lived process had a much higher amplitude in both cases, this time by a factor of approximately 20. The smaller 400 fs lifetime is likely due to vibrational cooling. The longer lifetime is harder to assign but is also likely due to hydrogen transfer. The species formed lives for a significantly shorter time than in alizarin-a, this could be due to instability of the hydrogen transfer state or proximity to a triplet state, resulting in intersystem crossing. The difference in lifetimes between the neutral and basic solutions is sufficiently small that it is, again, likely these are the same species. This further confirms that the species that is present in the acidic system is also present in the neutral system and is what is giving rise to the α excitation. Furthermore, the β excitation in the neutral system is likely the result of exciting the species found in the basic system. It also shows that it is unlikely that both alizarin-b and the monoanion are present as this would likely give rise to a higher number of exponentials required to fit the neutral species than the basic species, which is not the case.

Explicit solvent TDDFT calculations

While the experimental results already appear to rule out the tautomeric alizarin-b form, they are not able to provide a positive identification of which species is responsible for the secondary peak. To provide a clear differentiation between the two proposed tautomeric forms of the monoanion, we turn to theoretical spectroscopy.

To address this question, we use TDDFT to predict the excitation energies arising from

14

all of the proposed structures within a realistic model of the alizarin/methanol solution. As discussed, we find that the combination of explicitly-modelled solvent and a high-accuracy, though computationally costly, exchange-correlation functional such as a hybrid or range-separated hybrid is required for sufficient accuracy. We therefore use a simple spectral warping technique: we first use the semilocal PBE[33] functional to predict (at feasible computational cost) the excitations of a large ensemble of large snapshot models for each species, including explicit solvent. This is then followed by a warp of the resulting spectra to what would have been predicted had one of the more expensive functionals been used (in this case PBE0, LC-PBE0, B3LYP and CAM-B3LYP).[46–49] Since the spectra are dominated in each case by a single peak, the spectral warp required here is relatively simple: just a constant energy shift equal to the difference between the equivalent excitation energies for a given species calculated in the two functionals, within an implicit representation of the solvent. Applying this shift to all the excitation energies calculated for the snapshots in the less expensive functional in explicit solvent then results in a set of excitations mimicking a hypothetical set of calculations on the explicit solvent snapshots using the more expensive functional.

Figure 5 shows the results of implicit solvent calculations used to determine the shift parameter for each species, using the CAM-B3LYP shift as an example. It was observed that the predicted S_1 excitation energy for alizarin-a was 0.05 eV different from the observed experimental value when calculated using B3LYP. Furthermore, there was an observed error of 0.55eV in this predicted excitation from CAM-B3LYP. These errors are consistent with those observed by Anouar et $al.$, who, when utilizing an implicit PCM solvent model, also observed a large error associated with CAM-B3LYP; they found an error of 0.75 eV in this case as opposed to an error of just 0.15 eV when using B3LYP.[19]

As alizarin-a has already been confirmed as the source of the α excitation, a further small energy shift was applied to all the spectra for a given functional in order to align the theoretical and experimental peaks of the alpha excitation. The assumption underlying this

is that the error associated with the xc functional will have a similar value in each of these closely-related alizarin-derived species, allowing us to apply the same functional-dependent shift to all species. All the predicted explicit-solvent spectra were given a rigid shift of 0.05 eV (B3LYP), 0.15 eV (PBE0), 0.55 eV (CAM-B3LYP) and 0.95 eV (LC-PBE0) to produce the final comparison with experiment. The results are shown in Figure 6. After these shifts have been applied, the results between different functionals show a very high degree of consistency. It appears highly likely that the monoanion-b produces the β excitation and is thus the dominant second species, since in all four cases this species is closest to the observed position of the β excitation. The predicted position of alizarin-b is also close in several functionals, but it is unlikely this as evidenced by the previous experimental findings. Monoanion-a was a viable candidate following the experimental work, however it is significantly less likely given that the predicted peak is at least 75 nm away from the β excitation.
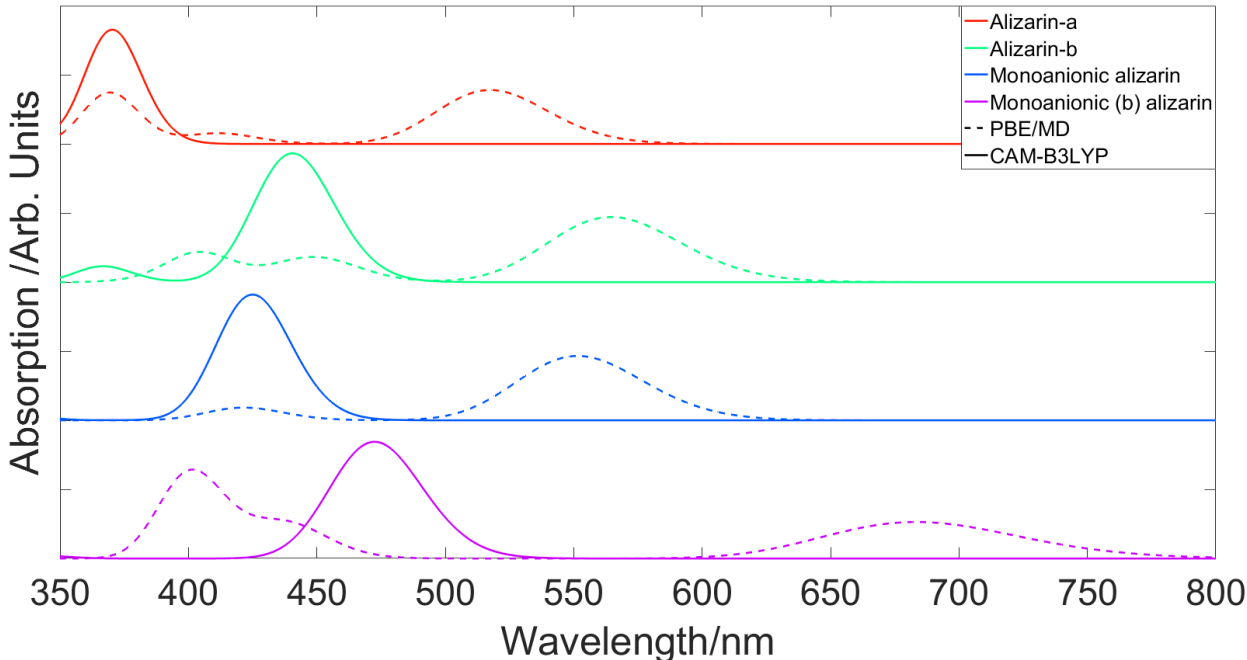

Figure 5: PBE and CAM-B3LYP calculations of forms of alizarin in implicit methanol solvent with 0.1 eV gaussian broadening, used for calculation of spectral warping parameters. These parameters are acquired through computing the difference between the PBE S_1 peak and the CAM-B3LYP S_1 peak.
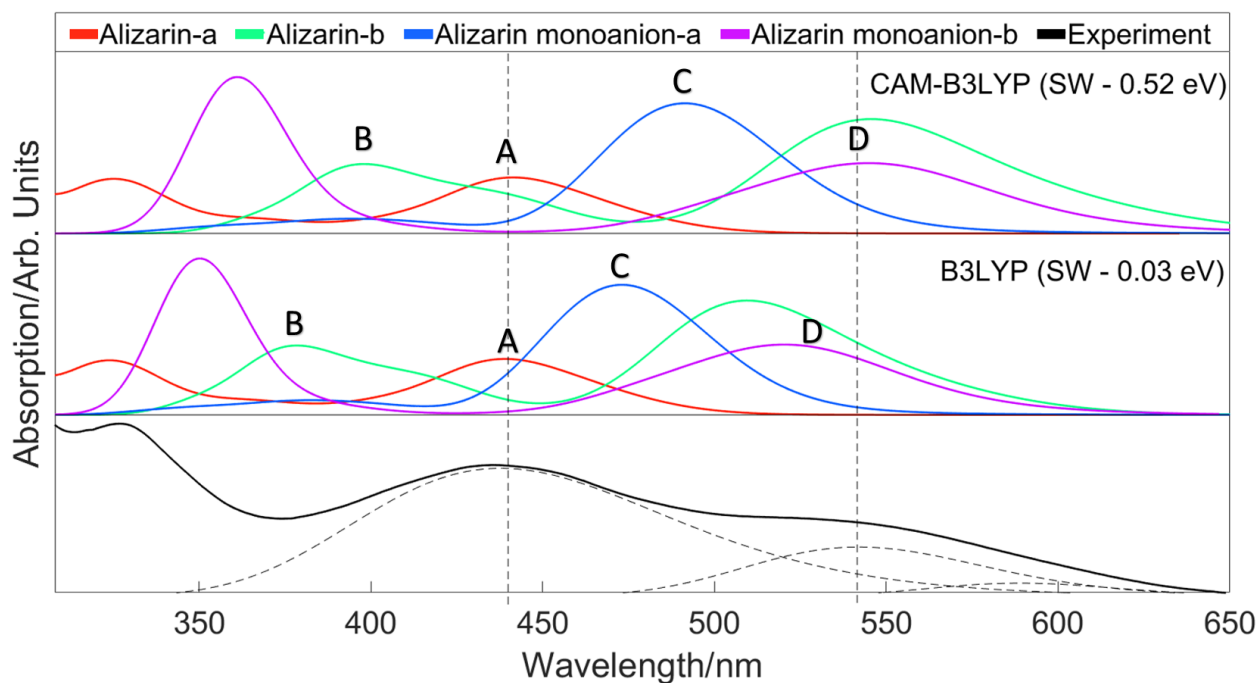
Figure 6: Predicted spectra for different forms of alizarin in explicit methanol solvent. A) Red is alizarin-a, B) green is alizarin-b, C) blue is alizarin monoanion-a; and D) pink is alizarin monoanion-b; the top panel shows the results of CAM-B3LYP spectral warp corrections. The middle panel shows the results of B3LYP spectral warp corrections. The bottom panel (black lines) shows the experimental spectra for comparison, with the main peaks deconvolved by fitting to gaussians.

This process was repeated with PBE0 and LC-PBE0 as the more expensive functionals, the results for this are shown in figure S4. Table 3 shows shifting parameter required to match the predicted S_1 excitation result for alizarin-a to the experimental value of α as well as the S_1 excitation of alizarin-b, monoanion-a, and monoanion-b post-shift.

Table 3: **Energy shifts required for each functional, to ensure the predicted S_1 excitation result for alizarin-a matches the experimental value of excitation α (435 nm). Also shown are the S_1 excitation wavelengths of alizarin-b, monoanion-a, and monoanion-b after the shift for each functional has been applied. For reference, the experimental value of the unknown β peak is 540 nm.**

Functional	Shift/ eV	Alizarin b /nm	Monoanion-a /nm	Monoanion-b /nm
B3LYP	0.03	513	476	525
CAM-B3LYP	0.52	526	491	548
PBE0	0.15	508	471	523
LC-PBE0	0.95	575	502	536

As previously discussed, Le Person *et al.* showed that the β excitation can be deconvolved into two gaussian peaks, and suggested that this was due to the presence of both a monoanionic species and the alizarin-b tautomer.[20] It can, however, be shown that the rotation of the dihedral angle associated with the OH bond in monoanion-b can shift the energy of the S_1 excitation. Figure 7 shows the range of UV-Vis absorption peaks associated with this rotation, as predicted by fixed-angle rotation calculations of alizarin in implicit methanol solvent; these were conducted using the cam-B3LYP functional. The range of absorption maxima caused by rotamers suggests that the broadness of the β excitation could be due to the rotation of this bond. The explicit solvent calculation for monoanion-b shows a broadened peak as well: this is due to the wide range of motion associated with this bond in the molecular dynamics snapshots.

We note also that in the explicit solvent spectra for monoanion-b, a higher-energy excitation at around 350-360 nm is predicted. In the experimental spectra which show the β-excitation we are now ascribing to monoanion-b, there is no clear evidence for that peak. However, the peak is in very close proximity to the higher-energy excitation of alizarin-a,

18

which the explicit solvent results seem to be predicting accurately. We thus presume these peaks are to some extent merging, resulting in the monoanion-b peak not being seen experimentally.
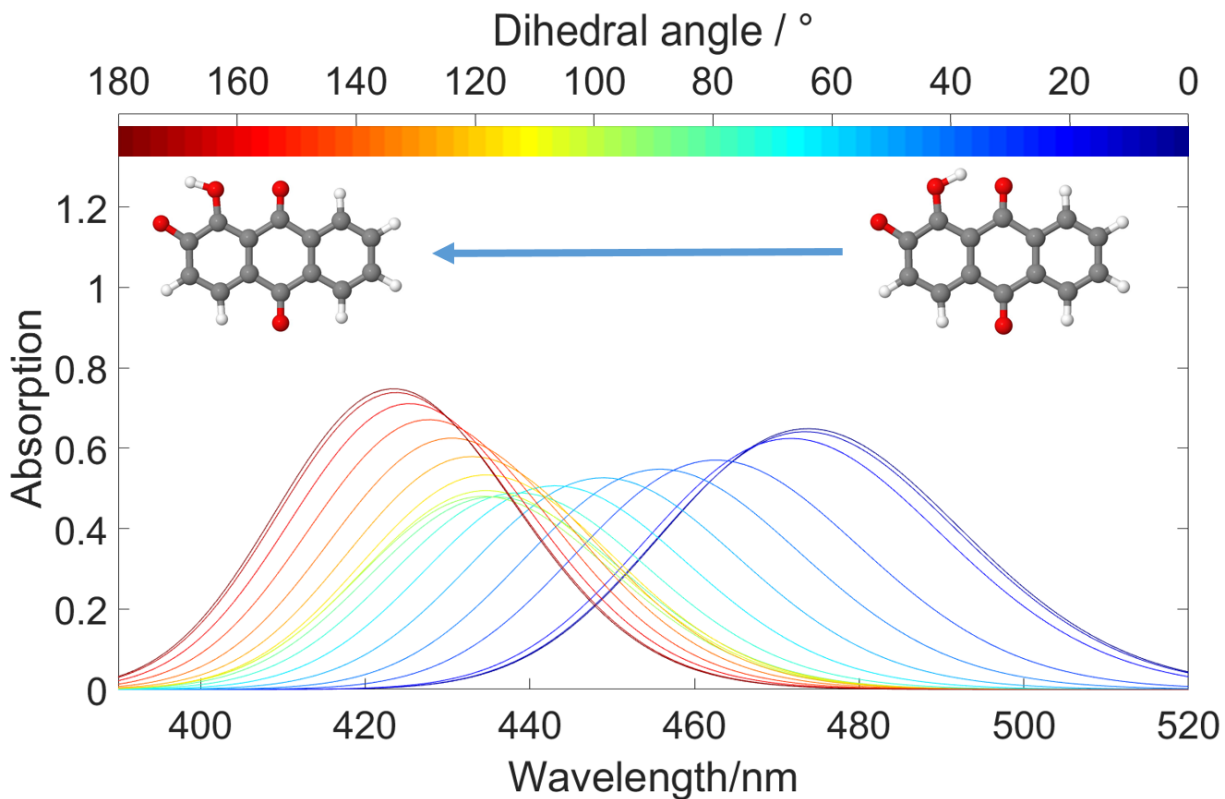

Figure 7: Range of predicted UV-Vis spectra for different rotamers of monoanionic alizarin-b, CAM-B3LYP/6-311G* implicit methanol PCM solvent.

Conclusions

The present work has provided a combination of methodologies appropriate to identifying secondary species in solvent. We apply this methodology to alizarin in methanol, and show that the most likely source of the secondary β excitation, at 540 nm, is monoanion-b form of alizarin. The broadness of this peak is likely due to the rotation of the alcohol group. In contrast to previous studies, we do not believe that alizarin-b is present, as evidenced by a number of observations: firstly, when acid is added to the system the peak completely disappears. It is unlikely the addition of acid would completely remove the alizarin-b tautomer. Secondly, in the transient absorption spectroscopy results we see a high degree of similarity between the TEAS spectrum for monoanionic alizarin and the TEAS spectrum for the β excitation. Both seem to have two excited state absorption peaks at 380 nm and 460 nm, and stimulated emission at 550 nm. This implies that in both cases, a monoanionic form of alizarin is being observed. The lack of any features unique to the TEAS data taken at neutral conditions with an excitation wavelength at 550 nm imply that alizarin-b is not being accessed.

We then proceed to show using theoretical calculations that the monoanion present is most likely to be monoanion-b. Using spectral-warping on explicit solvent calculations, we have demonstrated that monoanion-b has an excitation much closer in energy to the β peak than monoanion-a in all four considered functionals.

Desirable further work could include computational prediction of the excited state absorption and stimulated emission properties of monoanion-b, as well as monoanion-a and alizarin-b to further confirm the β excitation entirely arises from the former.

We propose that approaches to the identification of secondary species which are based solely on UV/vis-based methods and theoretical modelling would have strengths in addressing systems in dynamic equilibrium, specifically where the rate of conversion is sufficiently fast to preclude the use of NMR spectroscopy. It would also be advantageous in situations where there is no clear way to differentiate between candidate species using vibrational

spectroscopy. Such a situation occurs whenever there are overlapping absorption features between the solvent and solute, or between different functional groups on the solute.

The ability to identify photoactive equilibria samples in solution is of utmost importance in fields as wide ranging as dyes, sun protection, biological staining, and general organic synthesis. We feel this combination of methodologies offers a pathway to routinely identifying secondary species with considerably increased confidence.

Acknowledgement

Supporting Information Available

The Supporting Information contains the following plots:

- UV-Vis scans of alizarin in methanol at different temperatures.

- Fitted plots of TEAS slices of alizarin in methanol (pH=3,7), $\lambda(pu)$=425 nm , $\lambda(pr)$=500

nm.

- Fitted plots of TEAS slices of alizarin in methanol (pH=7,9), $\lambda(pu)$=550 nm , $\lambda(pr)$=460 nm.

- Predicted spectra for different forms of alizarin in methanol in PBE-based functionals.

- Solvent scans at $\lambda_{\mathrm{ex}} = 425$ nm, $\lambda_{\mathrm{pr}} = 500$ nm, in neutral and pH=3 methanol.

This material is available free of charge via the Internet at `http://pubs.acs.org/`.

References

(1) Antonov, L.; Nedeltcheva, D. Resolution of overlapping UV–Vis absorption bands and quantitative analysis. *Chem. Soc. Rev.* **2000**, *29*, 217–227.

(2) Antonov, L.; Gergov, G.; Petrov, V.; Kubista, M.; Nygren, J. UV–Vis spectroscopic and chemometric study on the aggregation of ionic dyes in water. *Talanta* **1999**, *49*, 99–106.

(3) Günther, M.; Wagner, E.; Ogris, M. Acrolein: unwanted side product or contribution to antiangiogenic properties of metronomic cyclophosphamide therapy? *J. Cell. Mol. Med.* **2008**, *12*, 2704–2716.

(4) Magde, D.; Rojas, G. E.; Seybold, P. G. Solvent dependence of the fluorescence lifetimes of xanthene dyes. *Photochem. and Photobiol.* **1999**, *70*, 737–744.

(5) Springer, V. G.; David Johnson, G. Use and advantages of ethanol solution of alizarin red S dye for staining bone in fishes. *Copeia* **2000**, *2000*, 300–301.

(6) Ovchinnikov, D. Alcian blue/alizarin red staining of cartilage and bone in mouse. *Cold Spring Harb Protoc* **2009**, *2009*, pdb–prot5170.

(7) Park, J.; Bauer, S.; Schlegel, K. A.; Neukam, F. W.; von der Mark, K.; Schmuki, P. TiO2 nanotube surfaces: 15 nm - an optimal length scale of surface topography for cell adhesion and differentiation. *Small* **2009**, *5*, 666–671.

(8) Szostek, B.; Orska-Gawrys, J.; Surowiec, I.; Trojanowicz, M. Investigation of natural dyes occurring in historical Coptic textiles by high-performance liquid chromatography with UV–Vis and mass spectrometric detection. *J. Chromatogr. A* **2003**, *1012*, 179–192.

(9) Moriguchi, T.; Yano, K.; Nakagawa, S.; Kaji, F. Elucidation of adsorption mechanism of bone-staining agent alizarin red S on hydroxyapatite by FT-IR microspectroscopy. *J. Colloid Interface Sci.* **2003**, *260*, 19–25.

(10) Douma, D. H.; M'Passi-Mabiala, B.; Gebauer, R. Optical properties of an organic dye from time-dependent density functional theory with explicit solvent: The case of alizarin. *J. Chem. Phys.* **2012**, *137*, 154314.

(11) Cysewski, P.; Jeliński, T.; Przybyłek, M.; Shyichuk, A. Color prediction from first principle quantum chemistry computations: a case of alizarin dissolved in methanol. *New J. Chem.* **2012**, *36*, 1836–1843.

(12) Miliani, C.; Romani, A.; Favaro, G. Acidichromic effects in 1, 2-di-and 1, 2, 4-trihydroxyanthraquinones. A spectrophotometric and fluorimetric study. *J. Phys. Org. Chem.* **2000**, *13*, 141–150.

(13) Zuehlsdorff, T. J.; Haynes, P. D.; Payne, M. C.; Hine, N. D. M. Predicting solvatochromic shifts and colours of a solvated organic dye: The example of nile red. *J. Chem. Phys.* **2017**, *146*, 124504.

(14) Preat, J.; Laurent, A. D.; Michaux, C.; Perpète, E. A.; Jacquemin, D. Impact of tautomers on the absorption spectra of neutral and anionic alizarin and quinizarin dyes. *J. Mol. Struct.: THEOCHEM* **2009**, *901*, 24–30.

(15) Jacquemin, D.; Perpete, E. A.; Scuseria, G. E.; Ciofini, I.; Adamo, C. TD-DFT performance for the visible absorption spectra of organic dyes: conventional versus long-range hybrids. *J. Chem. Theory Comput.* **2008**, *4*, 123–135.

(16) Savko, M.; Kaščáková, S.; Gbur, P.; Miškovskỳ, P.; Uličnỳ, J. Performance of time dependent density functional theory on excitations of medium sized molecules–Test on ionic forms of anthraquinone dihydroxy derivatives. *J. Mol. Struct.: THEOCHEM* **2007**, *823*, 78–86.

(17) Mech, J.; Grela, M. A.; Szaciłowski, K. Ground and excited state properties of alizarin and its isomers. *Dyes and Pigments* **2014**, *103*, 202–213.

(18) Dev, P.; Agrawal, S.; English, N. J. Determining the appropriate exchange-correlation functional for time-dependent density functional theory studies of charge-transfer excitations in organic dyes. *J. Chem. Phys.* **2012**, *136*, 224301.

(19) Anouar, E. H.; Osman, C. P.; Weber, J.-F. F.; Ismail, N. H. UV/Visible spectra of a series of natural and synthesised anthraquinones: experimental and quantum chemical approaches. *Springerplus* **2014**, *3*, 233.

(20) Le Person, A.; Cornard, J.-P.; Say-Liang-Fat, S. Studies of the tautomeric forms of alizarin in the ground state by electronic spectroscopy combined with quantum chemical calculations. *Chem. Phys. Lett.* **2011**, *517*, 41–45.

(21) Carta, L.; Biczysko, M.; Bloino, J.; Licari, D.; Barone, V. Environmental and complexation effects on the structures and spectroscopic signatures of organic pigments relevant to cultural heritage: the case of alizarin and alizarin–Mg (II)/Al (III) complexes. *Phys. Chem. Chem. Phys.* **2014**, *16*, 2897–2911.

(22) Zuehlsdorff, T. J.; Hine, N. D. M.; Spencer, J. S.; Harrison, N. M.; Riley, D. J.; Haynes, P. D. Linear-scaling time-dependent density-functional theory in the linear response formalism. *J. Chem. Phys.* **2013**, *139*, 064104.

(23) Zuehlsdorff, T. J.; Hine, N. D. M.; Payne, M. C.; Haynes, P. D. Linear-scaling time-dependent density-functional theory beyond the Tamm-Dancoff approximation: obtaining efficiency and accuracy with in situ optimised local orbitals. *J. Chem. Phys.* **2015**, *143*, 204107.

(24) Ge, X.; Timrov, I.; Binnie, S.; Biancardi, A.; Calzolari, A.; Baroni, S. Accurate and inexpensive prediction of the color optical properties of anthocyanins in solution. *J. Phys. Chem. A* **2015**, *119*, 3816–3822, PMID: 25830823.

(25) Casida, M. E.; Gutierrez, F.; Guan, J.; Gadea, F.-X.; Salahub, D.; Daudey, J.-P. Charge-transfer correction for improved time-dependent local density approximation excited-state potential energy curves: Analysis within the two-level model with illustration for H2 and LiH. *J. Chem. Phys.* **2000**, *113*, 7062–7071.

(26) Roberts, G. M.; Marroux, H. J.; Grubb, M. P.; Ashfold, M. N.; Orr-Ewing, A. J. On the participation of photoinduced N–H bond fission in aqueous adenine at 266 and 220 nm: a combined ultrafast transient electronic and vibrational absorption spectroscopy study. *J. Phys. Chem. A* **2014**, *118*, 11211–11225.

(27) Kimura, Y.; Alfano, J. C.; Walhout, P.; Barbara, P. F. Ultrafast transient absorption spectroscopy of the solvated electron in water. *J. Phys. Chem.* **1994**, *98*, 3450–3458.

(28) Greene, B.; Hochstrasser, R.; Weisman, R. Picosecond transient spectroscopy of molecules in solution. *J. Chem. Phys.* **1979**, *70*, 1247–1259.

(29) Greenough, S. E.; Horbury, M. D.; Thompson, J. O.; Roberts, G. M.; Karsili, T. N.; Marchetti, B.; Townsend, D.; Stavros, V. G. Solvent induced conformer specific photochemistry of guaiacol. *Phys. Chem. Chem. Phys.* **2014**, *16*, 16187–16195.

(30) Greenough, S. E.; Roberts, G. M.; Smith, N. A.; Horbury, M. D.; McKinlay, R. G.; Żurek, J. M.; Paterson, M. J.; Sadler, P. J.; Stavros, V. G. Ultrafast photo-induced

ligand solvolysis of cis-[Ru (bipyridine) 2 (nicotinamide) 2] 2+: experimental and theoretical insight into its photoactivation mechanism. *Phys. Chem. Chem. Phys.* **2014**, *16*, 19141–19155.

(31) Horbury, M.; Quan, W.-D.; Flourat, A.; Allais, F.; Stavros, V. Elucidating nuclear motions in a plant sunscreen during photoisomerization through solvent viscosity effects. *Phys. Chem. Chem. Phys.* **2017**, *19*, 21127–21131.

(32) Valiev, M.; Bylaska, E. J.; Govind, N.; Kowalski, K.; Straatsma, T. P.; Van Dam, H. J.; Wang, D.; Nieplocha, J.; Apra, E.; Windus, T. L. et al. NWChem: a comprehensive and scalable open-source solution for large scale molecular simulations. *Comp. Phys. Comms* **2010**, *181*, 1477–1489.

(33) Perdew, J. P.; Burke, K.; Ernzerhof, M. Generalized gradient approximation made simple. *Phys. Rev. Lett.* **1996**, *77*, 3865.

(34) Klamt, A.; Schüürmann, G. COSMO: a new approach to dielectric screening in solvents with explicit expressions for the screening energy and its gradient. *J. Chem. Soc., Perkin Transactions 2* **1993**, 799–805.

(35) York, D. M.; Karplus, M. A smooth solvation potential based on the conductor-like screening model. *J. Phys. Chem. A* **1999**, *103*, 11060–11079.

(36) Winget, P.; Dolney, D. M.; Giesen, D. J.; Cramer, C. J.; Truhlar, D. G. Minnesota solvent descriptor database. *Dept. of Chemistry and Supercomputer Inst., University of Minnesota, Minneapolis, MN* **1999**, *55455*.

(37) Case, D. A.; Berryman, J. T.; Betz, R. M.; Cerutti, D. S.; Cheatham III, T. E.; Darden, T. A.; Duke, R. E.; Giese, T. J.; Gohlke, H.; Goetz, A. W. et al. AMBER 2015. **2015**, University of California, San Francisco.

(38) Wang, J.; Wang, W.; Kollman, P. A.; Case, D. A. Automatic atom type and bond type perception in molecular mechanical calculations. *J. Mol. Graph.* **2006**, *25*, 247–260.

(39) Wang, J.; Wolf, R. M.; Caldwell, J. W.; Kollman, P. A.; Case, D. A. Development and testing of a general amber force field. *J. Comput. Chem.* **2004**, *25*, 1157–1174.

(40) Zuehlsdorff, T. J.; Haynes, P. D.; Hanke, F.; Payne, M. C.; Hine, N. D. M. Solvent effects on electronic excitations of an organic chromophore. *J. Chem. Theory Comput.* **2016**, *12*, 1853–1861.

(41) Dziedzic, J.; Helal, H. H.; Skylaris, C.-K.; Mostofi, A. A.; Payne, M. C. Minimal parameter implicit solvent model for ab initio electronic-structure calculations. *EPL (Europhys Lett)* **2011**, *95*, 43001.

(42) Lever, G.; Cole, D. J.; Hine, N. D. M.; Haynes, P. D.; Payne, M. C. Electrostatic considerations affecting the calculated HOMO–LUMO gap in protein molecules. *J. Phys.: Condensed Matter* **2013**, *25*, 152101.

(43) Skylaris, C.-K.; Haynes, P. D.; Mostofi, A. A.; Payne, M. C. Introducing ONETEP: Linear-scaling density functional simulations on parallel computers. *J. Chem. Phys.* **2005**, *122*, 084119.

(44) Ratcliff, L. E.; Hine, N. D. M.; Haynes, P. D. Calculating optical absorption spectra for large systems using linear-scaling density functional theory. *Phys. Rev. B* **2011**, *84*, 165131.

(45) Lee, S.; Lee, J.; Pang, Y. Excited state intramolecular proton transfer of 1, 2-dihydroxyanthraquinone by femtosecond transient absorption spectroscopy. *Current Applied Physics* **2015**, *15*, 1492–1499.

(46) Adamo, C.; Barone, V. Toward reliable density functional methods without adjustable parameters: The PBE0 model. *J. Chem. Phys.* **1999**, *110*, 6158–6170.

(47) Rohrdanz, M. A.; Herbert, J. M. Simultaneous benchmarking of ground-and excited-state properties with long-range-corrected density functional theory. *J. Chem. Phys.* **2008**, *129*, 034107.

(48) Becke, A. D. Density-functional thermochemistry. III. The role of exact exchange. *J. Chem. Phys.* **1993**, *98*, 5648–5652.

(49) Yanai, T.; Tew, D. P.; Handy, N. C. A new hybrid exchange–correlation functional using the Coulomb-attenuating method (CAM-B3LYP). *Chem. Phys. Lett.* **2004**, *393*, 51–57.

Graphical TOC Entry